

Monte Carlo study on the imaging performance of powder $\text{Lu}_2\text{SiO}_5:\text{Ce}$ phosphor screens under x-ray excitation: Comparison with $\text{Gd}_2\text{O}_2\text{S}:\text{Tb}$ screens

Panagiotis F. Liaparinis

Department of Medical Physics, Faculty of Medicine, University of Patras, 265 00 Patras, Greece

Ioannis S. Kandarakis and Dionisis A. Cavouras

Department of Medical Instruments Technology, Technological Educational Institute, 122 10 Athens, Greece

Harry B. Delis and George S. Panayiotakis^{a)}

Department of Medical Physics, Faculty of Medicine, University of Patras, 265 00 Patras, Greece

(Received 18 December 2006; revised 23 February 2007; accepted for publication 19 March 2007; published 24 April 2007)

$\text{Lu}_2\text{SiO}_5:\text{Ce}$ (LSO) scintillator is a relatively new luminescent material which has been successfully applied in positron emission tomography systems. Since it has been recently commercially available in powder form, it could be of value to investigate its performance for use in x-ray projection imaging as both physical and scintillating properties indicate a promising material for such applications. In the present study, a custom and validated Monte Carlo simulation code was used in order to examine the performance of LSO, under diagnostic radiology (mammography and general radiography) conditions. The Monte Carlo code was based on a model using Mie scattering theory for the description of light attenuation. Imaging characteristics, related to image brightness, spatial resolution and noise of LSO screens were predicted using only physical parameters of the phosphor. The overall performance of LSO powder phosphor screens was investigated in terms of the: (i) quantum detection efficiency (ii) emitted K-characteristic radiation (iii) luminescence efficiency (iv) modulation transfer function (v) Swank factor and (vi) zero-frequency detective quantum efficiency [DQE(0)]. Results were compared to the traditional rare-earth $\text{Gd}_2\text{O}_2\text{S}:\text{Tb}$ (GOS) phosphor material. The relative luminescence efficiency of LSO phosphor was found inferior to that of GOS. This is due to the lower intrinsic conversion efficiency of LSO (0.08 instead of 0.15 of GOS) and the relatively high light extinction coefficient m_{ext} of this phosphor ($0.239 \mu\text{m}^{-1}$ instead of $0.218 \mu\text{m}^{-1}$ for GOS). However, the property of increased light extinction combined with the rather sharp angular distribution of scattered light photons (anisotropy factor $g=0.624$ for LSO instead of 0.494 for GOS) reduce lateral light spreading and improve spatial resolution. In addition, LSO screens were found to exhibit better x-ray absorption as well as higher signal to noise transfer properties in the energy range from 18 keV up to 50.2 keV (e.g. DQE(0)=0.62 at 18 keV and for 34 mg/cm^2 , instead of 0.58 for GOS). The results indicate that certain optical properties of LSO (optical extinction coefficient, scattering anisotropy factor) combined with the relatively high x-ray coefficients, make this material a promising phosphor which, under appropriate conditions, could be considered for use in x-ray projection imaging detectors. © 2007 American Association of Physicists in Medicine. [DOI: [10.1118/1.2724065](https://doi.org/10.1118/1.2724065)]

Key words: radiation detectors, LSO, phosphor screens, Monte Carlo

I. INTRODUCTION

Three types of detector configurations are employed in modern flat panel digital radiology imagers: (a) indirect detectors based on a granular phosphor screen (e.g., $\text{Gd}_2\text{O}_2\text{S}:\text{Tb}$) to convert x-rays into light, (b) indirect detectors based on a phosphor screen of columnar structure (e.g., $\text{CsI}:\text{Tl}$) and (c) detectors using direct x-ray converters with charge collection in an electric field (e.g., *a*-Se detectors).¹⁻³ The indirect detector's performance (i.e., conversion of x rays into light and subsequently conversion of light into electrons) may be optimized either by improving the screen's structural param-

eters (e.g., grain size, packing density, thickness) or by employing new phosphor materials of improved physical characteristics (e.g., x-ray absorption efficiency, intrinsic conversion efficiency, emitted light spectrum).

Cerium doped lutetium orthosilicate- $\text{Lu}_2\text{SiO}_5:\text{Ce}$ (LSO) is a fluorescent material that was initially introduced by Melcher and Schweitzer as a single-crystal scintillator for positron emission tomographic (PET) applications.⁴ It was thereby shown that LSO could be a promising material, due to the following physical properties: (a) the presence of the high atomic number Lutetium atom and (b) the high value of bulk density (7.4 g/cm^3) (Ref. 5). Despite its high cost and its intrinsic low level radioactivity, LSO crystals have been

successfully used in PET systems.² Many reports have been published examining LSO single-crystal scintillator properties. Of specific interest are studies dealing with the following issues: (a) comparison of LSO single-crystal scintillator's performance to other scintillators,^{4,6-8} (b) depth of interaction determination,^{9,10} (c) PET LSO detectors' time of flight¹¹ and (d) the effect of K -characteristic radiation.^{12,13} Recently, powder LSO (phosphor in granular form) has been commercially available.¹⁴ Hence an investigation of the imaging properties of powder LSO for application in x-ray medical imaging systems may be of interest.

In the present work, Monte Carlo techniques were employed to predict the imaging performance of LSO granular phosphor screens and to compare this material to the widely used $\text{Gd}_2\text{O}_2\text{S:Tb}$ (GOS) phosphor. The present study was carried out by employing a custom Monte Carlo program to develop a screen performance model.¹⁵ This model takes into account the phosphor's optical properties (e.g., complex refractive index, light wavelength, x-ray to light conversion efficiency) as well as the structural properties of screens (e.g., grain size, packing density). Based on these characteristics, the model can predict the x-ray absorption, the light emission efficiency as well as the spatial resolution properties of a phosphor screen, under several conditions (e.g., x-ray energy, phosphor thickness).

Various parameters such as: (a) The quantum detection efficiency (QDE), (b) the energy absorption efficiency (EAE), (c) the luminescence efficiency (LE), (d) the modulation transfer function (MTF), (e) the Swank factor (SF) and (f) the detective quantum efficiency [DQE(0)] were evaluated and employed for comparison of the two phosphor materials (LSO and GOS). Additionally, data concerning the K -characteristic radiation emission were estimated. Both mammographic and general radiographic conditions (x-ray energy, screen thickness) were considered.

II. MATERIALS AND METHODS

The performance of a granular phosphor material is associated with the principal properties of phosphor screens, i.e., quantum efficiency, light creation and emission efficiency, spatial resolution and noise characteristics.¹ Detector's sensitivity is estimated by evaluating the quantum detection efficiency as well as the luminescence efficiency. The spatial resolution and noise characteristics are investigated by evaluating the modulation transfer function, the Swank factor and the detective quantum efficiency. To estimate these metrics, the present simulation, concerning GOS and LSO phosphor materials, took into consideration phosphor grain size and packing density, $7\ \mu\text{m}$ and 50%, respectively. For comparison purposes, results were obtained for equal screen thickness and x-ray energy. Table I shows data, relevant to the intrinsic physical properties of LSO and GOS, used in the present study.

TABLE I. Physical and scintillating properties of $\text{Lu}_2\text{SiO}_5\text{:Ce}$ and $\text{Gd}_2\text{O}_2\text{S:Tb}$.

	$\text{Lu}_2\text{SiO}_5\text{:Ce}$	$\text{Gd}_2\text{O}_2\text{S:Tb}$
Density (g/cm^3)	7.4 ^a	7.34 ^d
K -edge (keV)	63.44	50.30
Intrinsic efficiency	0.08 ^b	0.150 ^d
Emission peak (nm)	420 ^c	545 ^e
Index of refraction (real part)	1.82 ^a	2.30 ^f

^aReference 4.

^bReference 18.

^cReference 2.

^dReference 19.

^eReference 28.

^fReference 15.

A. Quantum detection efficiency (QDE) and energy absorption efficiency (EAE)

The QDE expresses the fraction of incident x-ray photons detected by a phosphor screen:¹

$$\text{QDE}(E, T) = 1 - \exp\left[-\frac{\mu(E)\rho_P T}{\rho}\right], \quad (1)$$

where $\mu(E)/\rho$ is the mass attenuation coefficient of the phosphor material, ρ_P is the packing density and T is the phosphor screen's coating thickness. Commercial screens used in x-ray medical imaging are usually prepared with thickness ranging from 10 up to 200 mg/cm^2 (lower values correspond to low sensitivity screens while higher values correspond to low resolution screens). In the present study two thickness values were considered: 34 mg/cm^2 corresponding to x-ray mammography and 60 mg/cm^2 corresponding to general x-ray radiography.¹⁶ QDE was estimated as the fraction of incident x-ray photons interacting within the screen. In this case, for energies lower than the K -shell binding energy, QDE is slightly higher than EAE. When an x-ray undergoes scattering and then escapes the screen, this event is taken into account in QDE evaluation while it is not included in the estimation of EAE. The latter is defined as the fraction of x-ray energy absorbed locally at the points of primary photon interactions within the phosphor mass.¹⁵ However, the net amount of energy deposited in the screen is generally affected by: (a) the energy loss when an x-ray photon undergoes inelastic scattering and escapes the phosphor mass and (b) the energy absorbed within the screen through K x rays after the K -fluorescence emission.

B. Luminescence efficiency (LE)

The LE is often ascribed to the ratio of light output over the amount of radiation incident on a phosphor or a scintillator^{17,18} and is related to the sensitivity of the medical imaging system.¹ It may concern either photon counting or energy integrating detectors. In the latter case, the definition of the LE can be given according to the following equation:

$$LE = \frac{\Psi_\lambda(E)}{\Psi_x(E)}, \quad (2)$$

where $\Psi_\lambda(E)$ is the light energy fluence emitted by the phosphor material and $\Psi_x(E)$ is the incident x-ray energy fluence. $\Psi_\lambda(E)$ may be evaluated by taking into account the phosphor's optical spectrum $S_p(E_\lambda)$ (i.e., number of light photons per energy interval). In such a case $\Psi_\lambda(E)$ may be expressed as follows:

$$\Psi_\lambda(E) = \int_{E_{\lambda_2}}^{E_{\lambda_1}} S_p(E_\lambda) E_\lambda dE_\lambda, \quad (3)$$

where E_λ is the light photon energy. However, it has previously been assumed that, if monochromatic emission is considered, the resulting error is less than 5% (Ref. 19). Hence all light photons may be considered to have equal energy, $E_\lambda = E_\lambda$, i.e., the mean spectrum energy \bar{E}_λ (Ref. 15). In this case, the light fluence is obtained by multiplying the number of the emitted light photons (N_λ) by their mean energy. N_λ is the number of light photons escaping the screen, either in reflection (from the x-ray irradiated surface) or in transmission mode (non irradiated surface). The incident x-ray energy fluence, $\Psi_x(E)$, is expressed by the following equation:

$$\Psi_x(E) = \int_0^{E_0} N_x(E) E dE, \quad (4)$$

where E_0 is the maximum spectral energy and $N_x(E)$ is the x-ray energy spectrum. The contribution of the principal intrinsic physical processes on the overall luminescence efficiency of a phosphor screen has been expressed by the following relation:^{17,20}

$$LE(E, T) = n_A(E, T) \eta_c G_L(E, T), \quad (5)$$

where n_A is the absorption efficiency (i.e., corresponding to the total energy deposited within the screen), η_c is the intrinsic x-ray to light conversion efficiency, expressing the fraction of absorbed x-ray energy that is converted into light in the phosphor material¹⁸ and G_L is the light transmission efficiency, i.e., the fraction of light produced that reaches the screen output.²⁰ G_L also expresses how efficiently light propagates through the phosphor mass. Light propagation depends on the interactions of light photons with the phosphor grains and on the direction that light photons follow after a scattering event. In the present Monte Carlo study, this information was described based on the Mie scattering theory^{15,21–23} according to the following considerations. Light absorption and light scattering coefficients $m_{\text{abs}}, m_{\text{sct}}$ are expressed in terms of the absorption (Q_{abs}) and scattering (Q_{sct}) efficiency factors as follows:¹⁵

$$m_{\text{abs}} = V_d A Q_{\text{abs}} \quad \text{and} \quad m_{\text{sct}} = V_d A Q_{\text{sct}}, \quad (6)$$

where V_d is the volume density of the phosphor material and A is the geometrical cross section of the grain. The latter depends on the diameter of the grain d being equal to $A = \pi d^2/4$. The corresponding absorption Q_{abs} and scattering Q_{sct} efficiency factors are given by the following expressions:^{15,21–23}

$$Q_{\text{ext}} = \frac{2}{x^2} \sum_{n=1}^{\infty} (2n+1) \text{Re}(a_n + b_n), \quad (7)$$

$$Q_{\text{sct}} = \frac{2}{x^2} \sum_{n=1}^{\infty} (2n+1) (|a_n|^2 + |b_n|^2),$$

where a_n and b_n are the so-called Mie coefficients, which are given as follows:²¹

$$a_n = \frac{\psi'_n(mx) \psi_n(x) - m \psi_n(mx) \psi'_n(x)}{\psi'_n(mx) \zeta_n(x) - m \psi_n(mx) \zeta'_n(x)}, \quad (8)$$

$$b_n = \frac{m \psi'_n(mx) \psi_n(x) - \psi_n(mx) \psi'_n(x)}{m \psi'_n(mx) \zeta_n(x) - \psi_n(mx) \zeta'_n(x)},$$

where $\psi_n(x)$ and $\zeta_n(x)$ are the Riccati-Bessel functions,^{15,21,22} x is the size parameter of Mie theory (equal to $x = \pi d n_{\text{medium}}/\lambda$), m is the relative complex refractive index (equal to $m = n_{\text{grain}}/n_{\text{medium}}$), λ is the wavelength of light, n_{grain} is the complex refractive index of the phosphor grains and n_{medium} is the refractive index of the binding material.

C. Modulation transfer function (MTF)

The modulation transfer function (MTF) expresses the signal transfer characteristics of an intensifying screen. The shape of the MTF curve is affected by the depth of x-ray interaction, which in turn affects the spatial distribution of the points of light creation within the phosphor.¹⁹ The relative depth distribution of the absorbed x-ray energy depends on the effective atomic number as well as on the density of the material. The contribution of scattering events, both elastic and inelastic, is also included in the aforementioned consideration.²⁴

In addition to x-ray penetration, the role of light propagation is also of crucial importance since it determines the spatial distribution of the emitted light. Light propagation depends on the light photon interaction effects,^{15,23,25,26} discussed in the previous section (see Sec. II B). A key parameter in the interpretation of MTF is the new direction of the scattered light photon, which is also affected by the size of phosphor grains, the light wavelength and phosphor's refractive index. In the present study the new light photon direction was expressed through the so-called anisotropy factor g . In this case, the new polar angle of the light photon is obtained according to Henyey–Greenstein distribution,^{15,27} as given below

$$\cos \theta = \frac{1}{2g} \left[1 + g^2 - \left(\frac{1 - g^2}{1 - g + 2gR} \right)^2 \right] \quad \text{when } g \neq 0, \quad (9)$$

where $\cos \theta$ is the cosine of the polar angle θ , R is a random number, and the free parameter g is the anisotropy factor, which implies isotropic distribution of light for $g=0$ and sharply forward direction of light for $g=1$ (Ref. 15). The anisotropy factor was calculated using the following equation:^{21,27}

$$g = \frac{\int_0^{\pi} 2\pi S_{11}(\theta) \cos \theta \sin \theta d\theta}{\int_0^{\pi} 2\pi S_{11}(\theta) \sin \theta d\theta}, \quad (10)$$

where $S_{11}(\theta)$ is the first element of the Mueller matrix,^{15,21} which implies that light extinction is independent of the light polarization state.

The MTF metric expresses the spatial resolution characteristics of an imaging system. It is defined as the ratio of the modulation of the output signal per the modulation of a sinusoidal input signal of the same frequency, given by²⁸

$$MTF(u) = \frac{|T(u)|}{T(0)}, \quad (11)$$

where the factor $T(u)$ is called the characteristic function of the system and $MTF(u)$ has by definition a value of unity at $u=0$.

To predict the MTF of a phosphor screen by our Monte Carlo simulation model, pencil beam geometry was employed. A two-dimensional point spread function (PSF) was then obtained by the optical photon distribution emitted by the screen (front side or backside). Then, the one-dimensional line spread function (LSF) along the x axis was obtained by integrating the PSF over one axis. The MTF curve was finally calculated by performing a fast Fourier transform of the LSF and normalizing its value to unity at zero spatial frequency.²⁸

D. Swank factor (SF) and detective quantum efficiency (DQE)

The DQE of an x-ray detector characterizes the system's overall signal-to-noise transfer properties.^{29,30} These properties are related to: (a) x-ray photon absorption at different interaction depths,¹⁹ (b) the fluctuations in the production of the optical photons³¹ (unequal number of light photons produced per absorbed x ray) and (c) the noise of the phosphor structure¹⁹ (grains of arbitrary size) affecting the fraction of emitted photons with respect to those produced. According to the above consideration, DQE is directly correlated with: (a) the x-ray detection efficiency η and (b) the statistical factor I , also known as Swank factor,³² which arises from the fluctuations in the number, m , of light photons emitted from the screen per absorbed x-ray photon. DQE was evaluated using the following formula:²⁹

$$DQE = \eta I, \quad (12)$$

where η represents the quantum detection efficiency (see Sec. II A) and I is the statistical factor determined by the following equation:

$$I = \frac{M_1^2}{M_0 M_2}, \quad (13)$$

where M_n is the n th moment of the light pulse height statistical distribution (statistical distribution of values of m) given as

$$M_n = \sum_m p(m) m^n, \quad (14)$$

where m is the number of light photons emitted from the screen per absorbed x-ray photon and $p(m)$ is the (pulse height) probability distribution giving the fluctuations in the number m (optical pulse).

For a given x-ray energy the Swank factor can be expressed as the product of two separate statistical factors, I_{OPD} and I_{AED} , as follows:³³

$$I = I_{OPD} I_{AED}, \quad (15)$$

where OPD stands for optical pulse distribution and AED stands for absorbed energy distribution, i.e., spectrum of absorbed energy per x-ray interaction event. In the present study a Poisson distribution¹⁹ was assumed for the production of light quanta per absorbed x-ray photon.

III. RESULTS AND DISCUSSION

The variation of QDE and EAE in the energy range from $E=18$ to $E=75$ keV is presented in Fig. 1, for two LSO and two GOS screens of 34 and 60 mg/cm². The LSO screens were found to have higher QDE and EAE values in a large part of the x-ray energy range considered. This is reasonable and may be explained on the basis of the higher density (ρ) and the higher effective atomic number (Z_{eff}) of LSO; e.g., the radiation detection index (ρZ_{eff}^A) (Ref. 2) is 147×10^{-6} for LSO compared to 103×10^{-6} for GOS. However, in the relatively narrow range between the corresponding K absorption levels, 50.3 keV for Gd and 63.4 keV for Lu respectively, both QDE and EAE were found higher for GOS. This is due to the effect of the K -level photoelectric absorption in Gd atoms. The increased QDE and EAE of LSO for energies above $E=63.4$ keV is also due to the same effect. However, the increased x-ray absorption after the K -absorption energy is followed by the production and emission of K -fluorescence x rays. This intrinsically produced radiation may either escape or be reabsorbed within the phosphor screen. In the first case, a fraction of the absorbed x-ray energy is lost, thus reducing detector sensitivity. This can be verified from the lower values of EAE with respect to QDE for all four cases shown in Fig. 1. In the second case (K -fluorescence reabsorption), image blurring occurs resulting in spatial resolution degradation.

In order to investigate the effect of K -fluorescence emission, the fraction (K_p) of K x rays escaping the screen (K photons escaping over K photons created) as well as the fraction (K_E) of energy absorbed via the reabsorption K -characteristic photons (K energy absorbed over incident x-ray energy) were determined. Results for these two parameters are shown in Table II. Both parameters were evaluated for the mean value of K_α and K_β -rays energy. In all cases the values corresponding to the LSO phosphor were found higher than those of GOS. This is due to: (i) The value of the K -fluorescence yield (ω_K), expressing the probability of K -photon creation over the probability of Auger electron emission, which is higher for Lu atoms (0.949 instead of

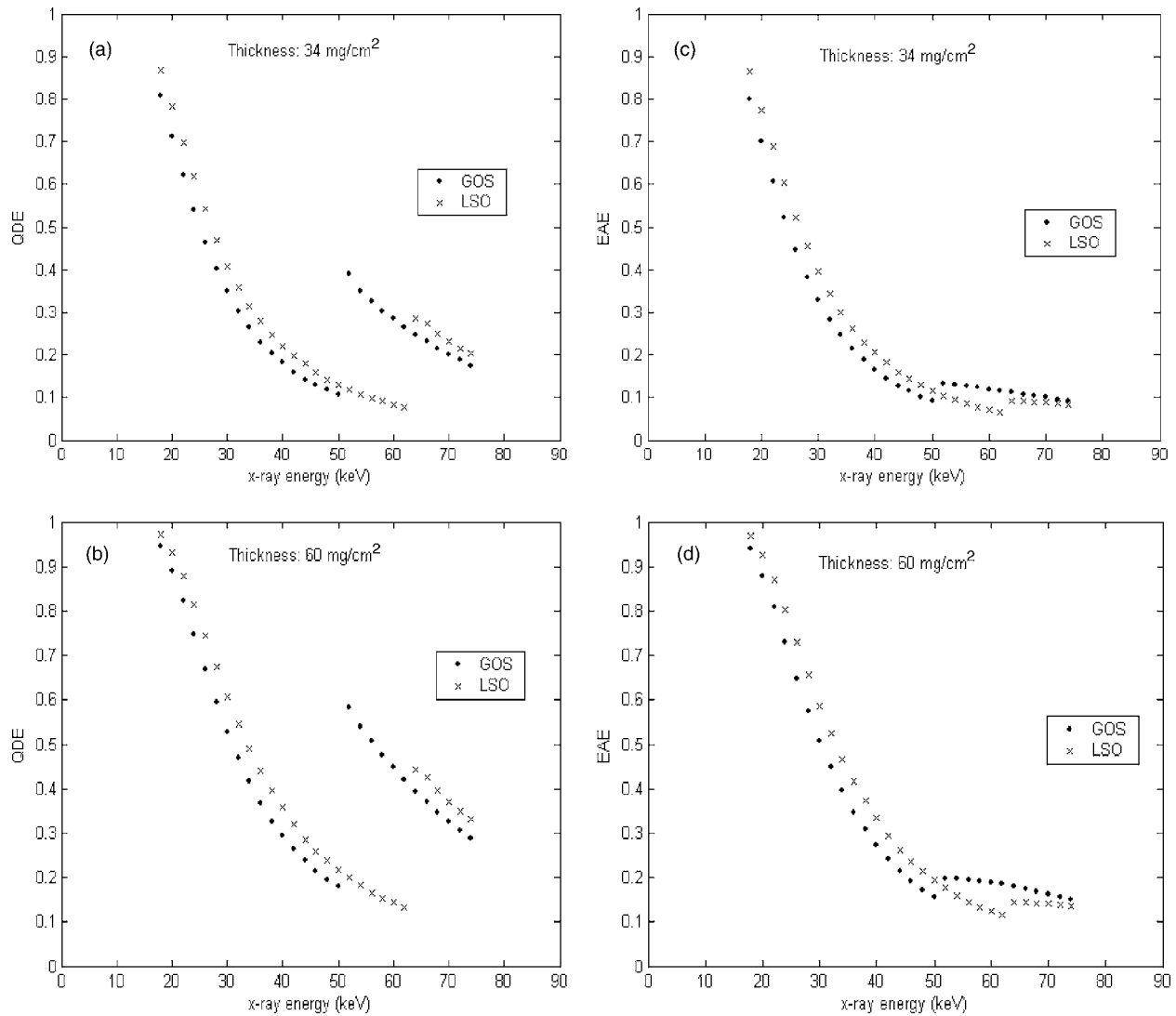


FIG. 1. The variation of QDE and EAE as a function of the incident x-ray energy (18–75 keV) for both GOS and LSO phosphor materials: (a) QDE for thickness: 34 mg/cm², (b) QDE for thickness: 60 mg/cm², (c) EAE for thickness: 34 mg/cm² and (d) EAE for thickness: 60 mg/cm².

0.932 of Gd atoms)³⁴ and (ii) the higher energy released in the Lu element through a K photon, ($E_{K\alpha}=E_K-E_{L2}=53.072$ keV and $E_{K\beta}=E_K-E_{L3}=54.199$ keV for Lu and $E_{K\alpha}=E_K-E_{L2}=42.356$ keV and $E_{K\beta}=E_K-E_{L3}=43.060$ keV for Gd), where E_K , E_{L2} and E_{L3} are the K -shell, L_2 -shell and L_3 -shell binding energies, respectively.

K_p factor was found to be higher for LSO than for GOS phosphor material because of the higher x-ray attenuation properties of the latter at the corresponding energy of K x rays. More specific, at $\bar{E}_{KL}=E_{K\alpha}+E_{K\beta}=42.71$ keV for GOS and $\bar{E}_{KL}=E_{K\alpha}+E_{K\beta}=53.64$ keV for LSO, the total mass at-

TABLE II. Comparison of (K_p) and (K_E) fractions between LSO and GOS phosphor materials for two different values (34 and 60 mg/cm²) of phosphor thickness.

X-ray energy (keV)	Thickness: 34 mg/cm ²				Thickness: 60 mg/cm ²			
	LSO		GOS		LSO		GOS	
	K_p %	K_E %	K_p %	K_E %	K_p %	K_E %	K_p %	K_E %
55	4.1	9.1
60	3.2	7.1
65	...	2.7	80.0	2.4	...	6.3	69.7	5.6
70	84.1	2.1	...	1.8	76.3	5.0	...	4.3
75	...	1.6	...	1.5	...	4.0	...	3.8

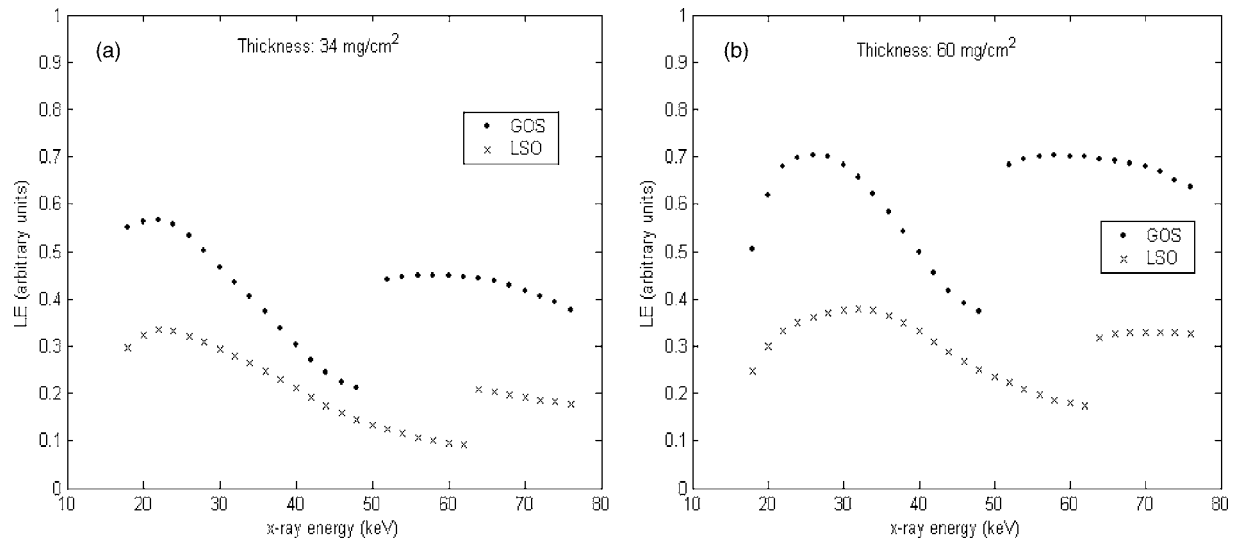


FIG. 2. The variation of LE as a function of the incident x-ray energy (18–75 keV) for both GOS and LSO phosphor materials: (a) thickness: 34 mg/cm², (b) thickness: 60 mg/cm².

tenation coefficient is equal to 4.927 and 3.420 cm²/g, respectively. This implies lower fraction of reabsorbed K x rays for LSO and therefore lower amount of K energy absorbed would be expected. However, the number of absorbed x rays above 63.4 keV, the number of K photons created per absorbed x-ray ($\omega_K=0.949$) as well as the amount of energy carried by the K photons ($\bar{E}_{KL}=53.64$ keV) is higher in LSO. Thus the amount of energy carried by K photons is larger contributing to higher values for K_E in LSO.

The LE with respect to the x-ray energy (from 18 up to 75 keV) is illustrated in Fig. 2. Results correspond to transmission mode configuration, i.e., light emission from the non irradiated backside of the screen. GOS phosphor screens were found to exhibit higher luminescence efficiency for both the 34 and the 60 mg/cm² thickness values. The LE differences between the two materials are due to following intrinsic physical processes: (i) The conversion of the absorbed x-ray energy into light energy within the phosphor material, which is expressed by the intrinsic x-ray to light conversion efficiency (η_c) and (ii) The light attenuation within the phosphor mass, which is expressed by the light extinction (absorption and scattering) coefficients [see Sec. III B, relation (6)]. For GOS, $\eta_c=0.15$. This value is higher than that of LSO ($\eta_c=0.08$) (Table 1). Hence, although LSO absorbs a higher fraction of the incident x-ray energy, the x-ray to light conversion process within this material produces light of lower intensity. This is mainly due to the forbidden energy band gap (E_G), between the valence and the conduction energy bands, which is larger in LSO, $E_G=6.4$ eV for LSO (Ref. 35) and $E_G=2.4$ eV for GOS (Ref. 28). Thus larger fractions of radiation energy are required to create electron-hole pairs (i.e., which are then captured by the activator and produce light) within the LSO phosphor. The aforementioned intrinsic scintillation mechanism may lead to afterglow emission which depends on the intensity and the duration of the incident radiation beam³⁶ as well as

on manufacturing techniques.³⁷ However, a complete investigation of afterglow would require a dedicated rigorous analysis, and thus it was not taken into account.

In addition, the light created within this material is significantly attenuated during light transport through the phosphor mass. This is principally due to the short light wavelength. This was verified by determining the light extinction coefficients within the framework of the Mie scattering theory and by taking into account the values of two optical parameters: (i) The mean wavelength of the emitted light ($\bar{\lambda}=420$ nm for LSO) and (ii) The real part of the refractive index ($n=1.82$ for LSO). Using these data as input values to the Mie theory based Monte Carlo algorithm,¹⁵ output values for the light extinction coefficients of the two materials were obtained [i.e., $m_{\text{ext}}=m_{\text{abs}}+m_{\text{sct}}$, where $m_{\text{abs}}, m_{\text{sct}}$ were taken from relation (6)]. For LSO phosphor the light extinction coefficient was found equal to $m_{\text{ext}}=0.239$ μm^{-1} which is higher than that obtained for GOS phosphor material ($m_{\text{ext}}=0.218$ μm^{-1}).

Figure 3 shows a comparison of MTF curves in transmission mode. Two different cases were evaluated: (a) phosphor thickness: 34 mg/cm², x-ray energy: 18 keV and (b) phosphor thickness: 60 mg/cm², x-ray energy: 49 keV. For both materials, MTF was found significantly better in the case of mammographic conditions (low thickness–low energy: 34 mg/cm², 18 keV). This is due to the following reasons: (a) light photons created within thin phosphor screens follow shorter trajectories to arrive at the screen surfaces, thus restricting light spread and resulting in narrow PSF, (b) the contribution of Compton scattering effect, within the phosphor, is less significant in the low energy case.

For the low thickness–low energy case (34 mg/cm², 18 keV) the MTF curve of the GOS phosphor screen was found to be superior than LSO. However, for the 60 mg/cm² phosphor thickness at 49 keV, the MTF of LSO screen was shown to be slightly superior than GOS. Since LSO exhibits

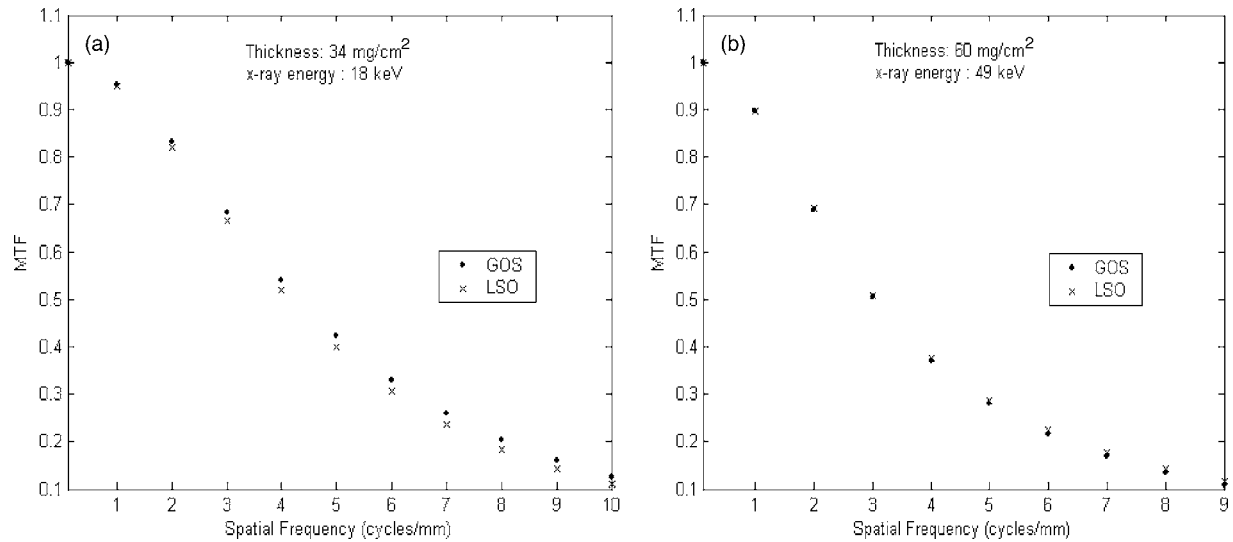


FIG. 3. The variation of MTF as a function of the spatial frequency for both GOS and LSO phosphor materials: (a) thickness: 34 mg/cm^2 , x-ray energy: 18 keV , (b) thickness: 60 mg/cm^2 , x-ray energy: 49 keV .

higher x-ray absorption, the depth distribution of absorbed x-ray energy is closer to the irradiated surface of the screen (x-ray beam entrance). This results in larger light spread giving broader PSF on the non irradiated output screen side (transmission mode). However, in the case of the thicker screen (i.e., 60 mg/cm^2), optical effects (i.e., light scattering, light absorption, light angular distribution) become more significant since the number of individual light photon interactions is larger. This may provide an advantage of LSO over GOS since, due to intrinsic optical properties, light diffusion is limited to lower solid angles within this phosphor.

This can be explained within the framework of the Mie scattering theory by taking into account the values of two optical parameters, i.e., the mean wavelength of the emitted light [$\bar{\lambda}=420 \text{ nm}$ for LSO), the real part of the refractive index ($n=1.82$ for LSO)] as well as the grain size considered ($7 \mu\text{m}$). Using our Monte Carlo model¹⁵ output values for the optical anisotropy factor [g in relation (9)] were obtained. The latter was found clearly higher for LSO (0.624 instead of 0.494 for GOS). Each time a light photon is scattered by a grain, the angle of its new trajectory is obtained via the Henyey-Greenstein distribution function (see Sec. II C). According to this distribution, higher values of anisotropy factor increase the probability of small angle scattering, as shown in Fig. 4. This implies a sharper angular distribution of light diffusion towards screen's output surface. Furthermore, the light absorption cross section of LSO was found to be slightly higher (approximately 1.16 times) than that of GOS. Hence light suffers higher attenuation within LSO phosphor, which is more important for the laterally directed light quanta. Thus lateral light spreading is of relatively lower significance in LSO screens.

Figure 5 provides the variation of SF with respect to x-ray energy, for LSO and GOS phosphor screens. SF is approximately equal for both phosphors for energies up to 50.2 keV . In the range from 50.2 up to 63.4 keV (between the K -edge

energies of Gd and Lu, respectively), SF was found much higher for the LSO. On the other hand, for energies higher than 63.4 keV , GOS was clearly better. These variations in SF may be explained by taking into account that for energies higher than 50.2 and 63.4 keV , for GOS and LSO respectively, the fluctuations in the number of the emitted optical photons become larger. This is due to the contribution of the K -fluorescence photons on the distribution of absorbed x-ray energy [corresponding to I_{AED} in relation (15)]. This distribution is modified since, for energies above the K edge of Gd and Lu, respectively, a fraction of the absorbed energy is lost, through the fraction of K x rays escaping the phosphor mass. This modification in the x-ray energy absorbed within the screen affects correspondingly the number of light quanta produced. This effect amplifies the fluctuations on the light

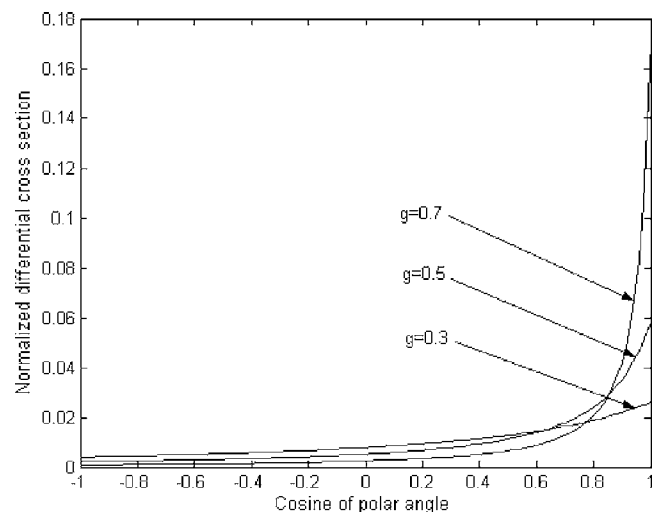


FIG. 4. The polar angle distribution of scattered light photons for different values of anisotropy factor g .

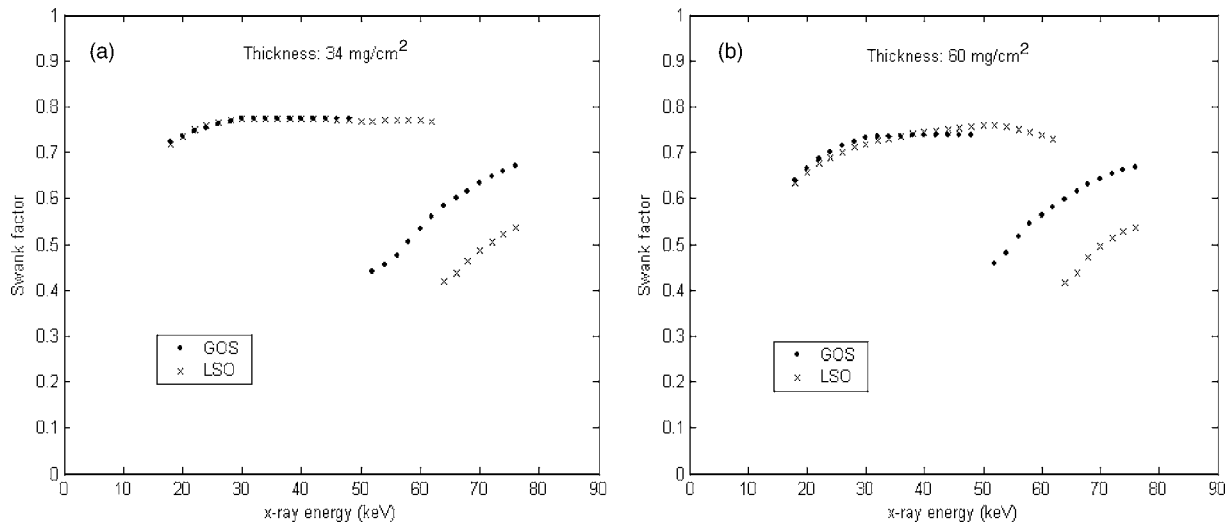


FIG. 5. The variation of Swank factor as a function of the incident x-ray energy (18–75 keV) for both GOS and LSO phosphor materials: (a) thickness: 34 mg/cm^2 , (b) thickness: 60 mg/cm^2 .

transmitted through the screen. Thus, the width of the optical pulse distribution is broadened resulting in larger values of M_2 .

The SF was found slightly higher for the 34 mg/cm^2 screen than for the 60 mg/cm^2 one. This provides an indication that SF is affected by phosphor thickness. This effect may be more clearly shown if screens of considerably different thicknesses are compared.^{33,38} Both I_{OPD} and I_{AED} factors [in Eq. (15)] are affected by screen thickness. However, compared to columnar screens,^{33,38} the contribution of the I_{OPD} factor in SF degradation is more significant in powder screens. This may be explained by taking into consideration that light absorption with respect to light scattering is affected by the screen's structure. In thick screens, the number of light photon interaction events increases. Light photons travel longer trajectories to escape the screen, thus interacting with a larger number of phosphor grains.³⁹ Thus the fluctuations in amplitudes of light pulses become larger causing a broadening in the optical pulse height distribution, which decreases SF.

DQE(0) values of both LSO and GOS phosphor materials are given in Table III. Up to the K edge, the variation of DQE(0) with incident photon energy is mainly affected by the x-ray absorption properties of the phosphor material in the corresponding x-ray energy, since Swank factor shows

very slight variations. As the incident x-ray energy increases, QDE of the phosphor decreases affecting DQE(0) in a similar way. Above the K edge, QDE increases suddenly and starts to decrease thereafter (see Fig. 1). On the other hand, SF shows a sudden drop and then increases with energy (see Fig. 4). DQE(0) values are affected by both the aforementioned variations [see Eq. (12)]; however, the impact of QDE on DQE variation seems to be more significant since DQE values decrease with energy after the K -absorption edge (Table III). LSO was found to have higher DQE(0) in the energy range from 18 up to 50.2 keV. These results may be of interest for mammographic applications as well as in microcomputed tomography applications.⁴⁰ In the latter case (i.e., x-ray energy: 40 keV), it may be of interest to note that the luminescence efficiency of LSO is close to that of GOS differing by 30% and 33.5% for phosphor thickness 34 and 60 mg/cm^2 , respectively.

Finally, it may be of significance to note that the accuracy of our results is subject to limitations related to: (a) the model's dependence on tabulated physical data (i.e., index of refraction) and on data drawn from the literature (i.e., light emission wavelength), (b) assumption of Poisson distribution for the production of light quanta per absorbed x-ray photon, (c) assumption for monochromatic light photons, (d) use of the common value (10^{-6}) for the imaginary part of the com-

TABLE III. DQE(0) data with respect to x-ray energy (18–75 keV). Comparisons between the two phosphor materials (LSO and GOS).

Phosphor material (thickness mg/cm^2)	Incident energy (keV)							
	18	22	32	49	51	63	64	75
	Detective quantum efficiency [DQE(0)]							
LSO (34)	0.62	0.52	0.28	0.10	0.09	0.06	0.12	0.11
GOS (34)	0.58	0.46	0.24	0.09	0.18	0.15	0.14	0.11
LSO (60)	0.62	0.60	0.40	0.17	0.16	0.09	0.18	0.17
GOS (60)	0.61	0.57	0.35	0.14	0.27	0.23	0.23	0.19

plex refractive index, (e) no reflection at the boundaries was considered, and (f) the effect of secondary electron range was not considered.

IV. CONCLUSION

In the present study the modeled performance of LSO powder phosphor screen was investigated for applications in mammography and general radiography. Investigation was performed using a custom Monte Carlo simulation program based on the Mie scattering theory for the description of light propagation. Within this treatment the results obtained for LSO phosphor were compared with results, determined under identical conditions, for the widely used GOS phosphor. Within the limitations and constraints of the present study (i.e., the accuracy of data available in the literature for the index of refraction and the light wavelength, the assumptions for monochromatic light emission, grain size, phosphor thickness, packing density, absence of absorbing dyes and reflective backing) the following conclusions can be drawn: (a) LSO phosphor material exhibits higher x-ray quantum detection and energy absorption efficiency within a large part of the diagnostic x-ray energy range, (b) the luminescence emission efficiency of LSO was found to be clearly lower than that of GOS. This is attributed to the lower intrinsic conversion efficiency of LSO (0.08) and to the higher light extinction coefficient ($0.239 \mu\text{m}^{-1}$), (c) The spatial resolution properties of LSO are comparable to GOS; GOS showed slightly better MTF in the thin screen low energy case (34 mg/cm^2 , 18 keV). For the thicker screen at higher energy (60 mg/cm^2 , 49 keV) LSO was slightly better. MTF and resolution properties are positively affected by the combined effects of lateral light extinction and forward directed angular distribution of scattering (anisotropy factor higher than 0.5, being 0.624 for LSO instead of 0.494 for GOS), (d) LSO shows higher signal to noise transfer properties especially at energies lower than the *K* edge of Gd element (50.2 keV). According to our Monte Carlo results, LSO could be employed in the design of medical x-ray detective systems, under the appropriate conditions (e.g., x-ray energy, phosphor thickness).

ACKNOWLEDGMENTS

The project is co-funded by the European Social Fund & National Resources-EPEAEK II-ARXIMIDIS.

^{a)} Author to whom correspondence should be addressed; electronic mail: panayiot@upatras.gr

¹ M. J. Yaffe and J. A. Rowlands, "X-ray detectors for digital radiography," *Phys. Med. Biol.* **42**, 1–39 (1997).

² C. W. E. van Eijk, "Inorganic scintillators in medical imaging," *Phys. Med. Biol.* **47**, R85–R106 (2002).

³ S. M. Gruner, M. W. Tate, and E. F. Eikenberry, "Charge-coupled device area x-ray detectors," *Rev. Sci. Instrum.* **73**, 2816–2842 (2002).

⁴ L. Melcher and J. S. Schweitzer, "Cerium-doped Lutetium Oxyorthosilicate: A fast, efficient new scintillator," *IEEE Trans. Nucl. Sci.* **39**, 502–505 (1992).

⁵ C. W. E. van Eijk, "Inorganic-scintillator development," *Nucl. Instrum. Methods Phys. Res. A* **460**, 1–14 (2001).

⁶ S. Weber, D. Christ, M. Kurzaja, R. Engels, G. Kemmerling, and H. Halling, "Comparison of LuYAP, LSO, and BGO as scintillators for high

resolution PET detectors," *IEEE Trans. Nucl. Sci.* **50**, 1370–1372 (2003).

⁷ J. Seidel, J. J. Vaquero, F. Barbosa, I. J. Lee, C. Cuevas, and M. V. Green, "Scintillator identification and performance characteristics of LSO and GSO PSPMT detector modules combined through common X and Y resistive dividers," *IEEE Trans. Nucl. Sci.* **47**, 1640–1645 (2000).

⁸ C. S. Levin, "Design of a high-resolution and high-sensitivity scintillation crystal array for PET with nearly complete light collection," *IEEE Trans. Nucl. Sci.* **49**, 2236–2243 (2002).

⁹ J. S. Huber, W. W. Moses, M. S. Andreaco, and O. Petterson, "An LSO scintillator array for a PET detector module with depth of interaction measurement," *IEEE Trans. Nucl. Sci.* **48**, 684–688 (2001).

¹⁰ C. W. Lerche, J. M. Benloch, F. Sanchez, N. Pavon, B. Escat, E. N. Gimenez, M. Fernandez, I. Torres, M. Gimenez, A. Sebastia, and J. Martinez, "Depth of γ -ray interaction within continuous crystals from the width of its scintillation light-distribution," *IEEE Trans. Nucl. Sci.* **52**, 560–572 (2005).

¹¹ W. W. Moses and S. E. Derenzo, "Prospects of time-of-flight PET using LSO scintillator," *IEEE Trans. Nucl. Sci.* **46**, 474–478 (1999).

¹² G. Zavattini, A. Del Guerra, N. Cesca, G. Di Domenico, M. Gambaccini, E. Moretti, and N. Sabba, "High Z and medium Z scintillators in ultra-high-resolution small animal PET," *IEEE Trans. Nucl. Sci.* **52**, 222–230 (2005).

¹³ P. Liaparinos, I. Kandarakis, D. Cavouras, H. Delis, and G. Panayiotakis, "Investigating the effect of *K*-characteristic radiation on the performance of nuclear medicine scintillators by Monte Carlo methods, *Nucl. Instrum. Methods Phys. Res. A* **569**, 364–367 (2006).

¹⁴ <http://www.phosphor-technology.com/products/scint.htm>

¹⁵ P. Liaparinos, I. Kandarakis, D. Cavouras, H. Delis, and G. Panayiotakis, "Modeling granular phosphor screens by Monte Carlo methods," *Med. Phys.* **33**, 4502–4514 (2006).

¹⁶ T. Yu, J. M. Sabol, J. A. Seibert, and J. M. Boone, "Scintillating fiber optic screens: A comparison of MTF, light conversion efficiency, and emission angle with Gd₂O₂S:Tb screens," *Med. Phys.* **24**, 279–285 (1997).

¹⁷ G. W. Ludwig, "X-ray efficiency of powder phosphors," *J. Electrochem. Soc.* **118**, 1152–1159 (1971).

¹⁸ G. Blasse, "The luminescent efficiency of scintillators for several applications: State-of-the-art," *J. Lumin.* **60**, **61**, 930–935 (1994).

¹⁹ R. M. Nishikawa and M. J. Yaffe, "Model of the spatial-frequency-dependent detective quantum efficiency of phosphor screens," *Med. Phys.* **17**, 894–904 (1990).

²⁰ I. Kandarakis, D. Cavouras, G. S. Panayiotakis, and C. D. Nomicos, "Evaluating x-ray detectors for radiographic applications: A comparison of ZnScdS:Ag with Gd₂O₂S:Tb and Y₂O₂S:Tb screens," *Phys. Med. Biol.* **42**, 1351–1373 (1997).

²¹ H. C. Van de Hulst, *Light Scattering by Small Particles* (Wiley, New York, 1957).

²² H. Du, "Mie-scattering calculation," *Appl. Opt.* **43**, 1951–1956 (2004).

²³ R. Morlotti, "X-ray efficiency and modulation transfer function of fluorescent rare earth screens, determined by the Monte Carlo method," *J. Photogr. Sci.* **23**, 181–189 (1975).

²⁴ G. E. Giakoumakis, C. D. Nomicos, and P. C. Euthimiou, "Modulation transfer function of fluorescent screens excited by x rays," *Phys. Med. Biol.* **25**, 1105–1110 (1980).

²⁵ G. E. Giakoumakis, M. C. Katsarioti, I. E. Lagaris, and G. S. Panayiotakis, "A theoretical model for the x-ray luminescence of granular phosphor screens," *J. Appl. Phys.* **69**, 6607–6610 (1991).

²⁶ J. Lindstrom and G. A. Carlsson, "A simple model for estimating the particle size dependence of absolute efficiency of fluorescent screens," *Phys. Med. Biol.* **44**, 1353–1367 (1999).

²⁷ V. G. Peters, D. R. Wyman, M. S. Patterson, and G. L. Frank, "Optical properties of normal and diseased human breast tissues in the visible and near infrared," *Phys. Med. Biol.* **35**, 1317–1334 (1990).

²⁸ M. J. Yaffe, "Physics and psychophysics," *Handbook of Medical Imaging*, edited by J. Beutel, H. L. Kundel, and R. L. Van Metter (SPIE, Washington, 2000), Chap. 5, Vol. I, pp. 329–372.

²⁹ C. E. Dick and J. W. Motz, "Image information transfer properties of x-ray fluorescent screens," *Med. Phys.* **8**, 337–346 (1981).

³⁰ N. T. Ranger, E. Samei, J. T. Dobbins, and C. E. Ravin, "Measurement of the detective quantum efficiency in digital detectors consistent with the IEC 62220-1 standard: Practical considerations regarding the choice of filter material," *Med. Phys.* **32**, 2305–2311 (2005).

³¹ J. Beutel, B. A. Apple, and R. Shaw, "The role of screen parameters and

- print-through in the performance of film/screen systems,” *Phys. Med. Biol.* **38**, 1181–1193 (1993).
- ³²R. K. Swank, “Absorption and noise in x-ray phosphors,” *J. Appl. Phys.* **45**, 4199–4203 (1974).
- ³³W. Zhao, G. Ristic, and J. A. Rowlands, “X-ray imaging performance of structured cesium iodide scintillators,” *Med. Phys.* **31**, 2594–2605 (2004).
- ³⁴J. H. Hubbell, P. N. Trehan, N. Singh, B. Chand, D. Mehta, M. L. Garg, R. R. Grag, S. Singh, and S. Puri, “A review, bibliography, and tabulation of K, L, and higher atomic shell x-ray fluorescence yields,” *J. Phys. Chem. Ref. Data* **23**, 339–364 (1994).
- ³⁵M. Kobayashi, M. Ishii, and C. L. Melcher, “Radiation damage of a cerium-doped lutetium oxyorthosilicate single crystal,” *Nucl. Instrum. Methods Phys. Res. B* **132**, 509–512 (1993).
- ³⁶A. G. Glendinning, S. G. Hunt, and D. E. Bonnett, “Measurement of the response of $\text{Gd}_2\text{O}_3\text{:Tb}$ phosphor to 6 MV x rays,” *Phys. Med. Biol.* **46**, 517–530 (2001).
- ³⁷J. G. Mainprize and M. J. Yaffe, “The effect of phosphor persistence on image quality in digital x-ray scanning systems,” *Med. Phys.* **25**, 2440–2454 (1998).
- ³⁸A. Badano, I. S. Kyprianou, and J. Sempau, “Anisotropic imaging performance in indirect x-ray imaging detector,” *Med. Phys.* **33**, 2698–2713 (2006).
- ³⁹M. Drangova and J. A. Rowlands, “Optical factors affecting the detective quantum efficiency of radiographic screens,” *Med. Phys.* **13**, 150–157 (1986).
- ⁴⁰G. Hajdok, J. Yao, J. J. Battista, and I. A. Cunningham, “Signal and noise transfer properties of photoelectric interactions in diagnostic x-ray imaging detectors,” *Med. Phys.* **33**, 3601–3620 (2006).